Advanced Review

Computational design of two-dimensional topological materials

Z. F. Wang,[1] Kyung-Hwan Jin[2] and Feng Liu[2,3]*

The progress in science and technology is largely boosted by the continuous discovery of new materials. In recent years, the state-of-art first-principles computational approach has emerged as a vital tool to enable materials discovery by designing *a priori* unknown materials as well as unknown properties of existing materials that are subsequently confirmed by experiments. One notable example is the rapid development of the field of topological materials, where new candidates of topological materials are often predicted and/or designed before experimental synthesis and characterization. Topological phases of condensed mater not only represent a significant advance in the fundamental understanding of material properties but also hold promising applications in quantum computing and spintronics. In this article, we will give an overview of recent progress in computational design of two-dimensional topological materials and an outlook of possible future research directions. © 2017 John Wiley & Sons, Ltd

How to cite this article:
WIREs Comput Mol Sci 2017, e1304. doi: 10.1002/wcms.1304

INTRODUCTION

Computational materials science is a highly interdisciplinary research field that encompasses theoretical methods developed in biology, chemistry, mathematics, physics, and engineering. A variety of computational methods at different length and time scales have been developed, ranging from electronic structure methods based on density functional theory (DFT),[1] molecular dynamics,[2] and Monte-Carlo techniques[3] to phase-field method[4] and continuum macroscopic approaches. While the foundations of most these computational methods are well established, the development of optimized algorithms is ongoing to enable the computation of increasingly complex materials and systems with improved accuracy and efficiency. Importantly, as the computational approaches become more and more powerful, the field of computational materials has steadily evolved from elucidating experimental results to making predictions to guide experiments, especially in predictive design of new materials with the latest development of materials discovery by computing and data mining.[5] It is highly expected that computational design will lead to discovery of many more new materials, as well as significant reduction of time and cost in materials research and industrial production.

In designing electronic/spintronic materials, the first-principles DFT computational methods have led the way. Given the (crystalline) atomic structures, the DFT methods are generally capable of predicting reliably the electronic, magnetic, and optoelectronic properties. One exciting example is the latest discovery of topological materials aided by computational design from first prinicples.[6–8] The first-principles computational design approaches have worked out as a powerful research tool in realizing theoretical (lattice) models of topological phases in real materials systems, outputting relevant properties that can be tested and confirmed directly by experiments. They have also served as valuable benchmarks for obtaining the parameters in semi-empirical methods,

*Correspondence to: fliu@eng.utah.edu

[1]Hefei National Laboratory for Physical Sciences at the Microscale, Synergetic Innovation Center of Quantum Information and Quantum Physics, CAS Key Laboratory of Strongly-Coupled Quantum Matter Physics, University of Science and Technology of China, Hefei, China

[2]Department of Materials Science and Engineering, University of Utah, Salt Lake City, UT, USA

[3]Collaborative Innovation Center of Quantum Matter, Beijing, China

Conflict of interest: The authors have declared no conflicts of interest for this article.

such as tight-binding methods, which allows one to reveal deeper physical insights of topological properties and better understand experimental results. It is worth noting that although exotic, most topological materials properties lie within the picture of single-particle band structure without the need of considering many-body effects. For this reason, standard DFT methods are reliable enough in predicting topological properties, including the 'gap' opened by spin-orbit coupling (SOC) which is usually much smaller than the conventional charge localization gap in semiconductors and insulators.

The field of topological materials started with discovery of topological insulators (TIs),[9–14] which have drawn much attention in recent years. To date, most TIs are first theoretically predicted or computationally designed, followed by experimental confirmation. Introducing the concept of topology in solid-state materials provides a new perspective for understanding the origin of different quantum phenomena. The two-dimensional (2D) TI, also called quantum spin Hall (QSH) insulators,[10,11] is closely related to the integer quantum Hall effect.[15,16] It has a bulk energy gap and a pair of gapless metallic edge states that are protected by the time reversal symmetry (TRS). Unlike any other 1D electronic systems, the conducting channels of these topological edge states are protected from elastic backscattering and localization, and hence hold potential applications in quantum computing and spintronics.

In this article, we attempt to give an up-to-date overview of the research progress in computational design of 2D TI materials. Some comprehensive reviews of 2D TI materials are already avaiable,[17] here we will focus on the computational design aspects of discovering new 2D TI materials, highlighting a few interesting systems studied most recently. We first discuss two discrete lattice models for 2D TIs, in terms of three design parameters of crystalline lattice symmetry, SOC, and atomic orbital composition. We then discuss two specific classes of 2D TI materials, designed based on the discrete lattice models and associated parameters. One is the organic 2D TI materials, including triphenyl-bismuth,[18] π-conjugated,[19] and Cu-dicyanoanthracene[20] frameworks. The other is the surface-based 2D TI materials supported on a substrate, including Bi-Cl/Si(111),[21] Au/GaAs(111),[22] and FeSe/$SrTiO_3$(001)[23] films. In addition, we briefly review some 2D TI materials involving d orbitals. Importantly, some of these candidate materials have already been synthesized in the experiments with their topological properties confirmed. Finally, we discuss briefly on possible future research directions in computational design of topological materials.

DESIGNING MODELS FOR 2D TIs

Topological insulators (TIs) are indexed by topological invariant Z_2 number,[12] which accounts for the number of times that electron wavefunctions exchange phases with their complex conjugates in traversing half of the Brillouin zone. In the presence of TRS, the topological invariant takes only two values. An odd number corresponds to Z_2 invariant $\nu = 1$, indicating a topological nontrivial phase, while an even number corresponds to $\nu = 0$, indicating a topological trivial phase. If a system has both TRS and inversion symmetry,[24] the Z_2 topological invariant can be computed simply by counting how many times the electron wavefunctions exchange their parity at the time reversal invariant momenta (TRIM). If the valence band exchanges parities odd number of times with the conduction band with opposite parity, it gives a nontrivial topological phase. The mechanism for parity inversion is not unique, and can vary with a wide range of tuning parameters. Among them, SOC is responsible for band inversion in most known TIs.[9–14] Therefore, in a general model, the Z_2 invariant servers as the defining parameter to design TI materials.

Based on the Z_2 theory, two prevailing lattice models have been developed providing the basic guiding principles to design 2D TI materials. In the first model, originally introduced by Kane and Mele (KM) in 2005,[9] the starting material is a semimetal of hexagonal lattice such as graphene. The valence and conduction bands touch with each other to form a Dirac band (Figure 1(a)), with the Fermi level lying at the Dirac point. The band order has already been inverted in this case, with the parity of the valence and conduction bands exchanged. Thus, any finite SOC will lift the band degeneracy and open a nontrivial SOC gap to turn the system into 2D TI. The band parity does not change during the gap opening process. This model corresponds to two copies of Haldane model[25] encoded with opposite spins and Chern number that generate a pair of gapless edge states within the SOC gap that counter-propagate along the edge with opposite spins, which are characteristic features of 2D TIs.

In the second model, originally introduced by Bernevig, Hughes, and Zhang (BHZ) in 2006,[10] the starting material is a narrow-gap semiconductor whose valence and conduction bands have opposite parities (Figure 1(b)), which has a trivial topological

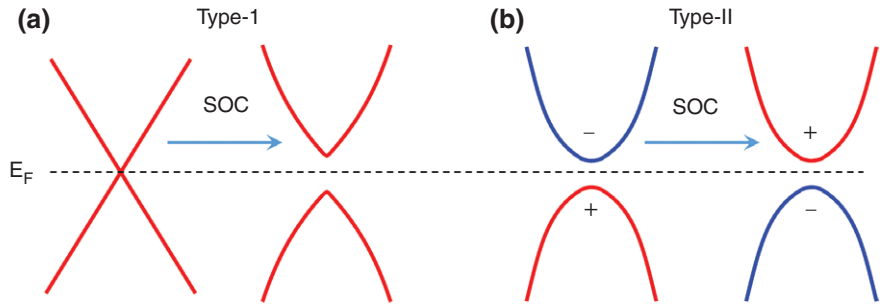

FIGURE 1 | Schematic band structures of two lattice models for designing two-dimensional topological insulator materials. (a) The first model with a spin-orbit coupling (SOC) induced band gap opening at the Dirac point. (b) The second model with an SOC induced band inversion between valence and conduction band with opposite parities. + and – labels even and odd parity. The dashed line denotes the Fermi level.

phase. By including SOC, the trivial band gap is first closed and then a nontrivial gap is opened, accompanied with a band inversion between the valence and conduction bands. This type of topological band structure is first derived from a square lattice in HgTe/CdTe quantum well system.[10] It was shown that HgTe/CdTe quantum well (a HgTe thin film sandwiched between two layers of conventional insulator of CdTe) will become a 2D TI when the thickness of HgTe is above a critical value.

The seminal works by KM and BHZ laid the groundwork for TIs. However, experimental realization of 2D TI has been challenging. For the KM model, graphene has too weak an SOC to behave as a TI with observable topological properties. Consequently, computational design efforts have been made to enhance the intrinsic SOC in graphene[26] or to search graphene-like materials with larger SOC.[27–35] However, no experiment has yet confirmed the KM model in a real material of hexagonal lattice using quantum transport measurement, although evidence of topological edge states have been shown by scanning tunneling spectroscopy (STS) measurement in Bi(111) bilayer grown on a substrate.[36–38] On the other hand, the BHZ model has been verified experimentally in two systems of HgTe/CdTe[11] and InAs/GaSb.[39] A quantized conductance ($2e^2/h$) in zero magnetic field is observed when the chemical potential of the sample is tuned into the bulk gap, giving the direct evidence for the gapless edge states in the nontrivial gap. However, the extremely low temperature for observing the topological phase greatly inhibits its further development and future applications. Therefore, there remains an intensive search for new 2D TIs to ease the experimental realization.

Based on the above two original models, there are three key ingredients for consideration in computational design of a 2D TI: lattice symmetry, SOC, and orbital composition around Fermi level. In choosing lattice symmetry, any 2D lattice that gives rise to a Dirac band can be a candidate to realize the KM-like model, to host TI state in presence of a finite SOC. For SOC, one simply chooses heavy elements in the bottom part of the periodic table in order to increase the gap opened by SOC. The choice of orbital composition is less apparent sometimes. If the band edge states are non-degenerate, then the valence and conduction band edge should be composed of one orbital each with opposite parity (odd vs even) so that a two-band inversion can be realized straightforwardly. If the band edge states are degenerate, the choices become more complex and additional model analysis is needed. We note that in general, different lattice models may be adiabatically connected to different classes of effective models of topological quantum field theory at the continuum limit, which requires only two-band inversion.[40] In addition, an intrinsic TI needs to have right number of electrons for a half-filled band, or electron or hole doping is need to move the Fermi energy to inside the SOC gap.

ORGANIC TOPOLOGICAL MATERIALS

To date, many topological materials have been predicted theoretically and confirmed experimentally, especially for the 3D materials.[41–46] However, most of them are based on inorganic materials. Historically, however, inorganic materials and devices have always found their organic counterparts, such as organic semiconductors and superconductors. In general, organic materials have the added advantages of low cost, easy fabrication, and mechanical flexibility. Meanwhile, advances on synthetic chemistry and nanotechnology have shown the potential in producing complex 2D lattices, that is, covalent organic frameworks (COFs). This has motivated recent computational design of a series of 2D organic topological materials.[18–20,47–56]

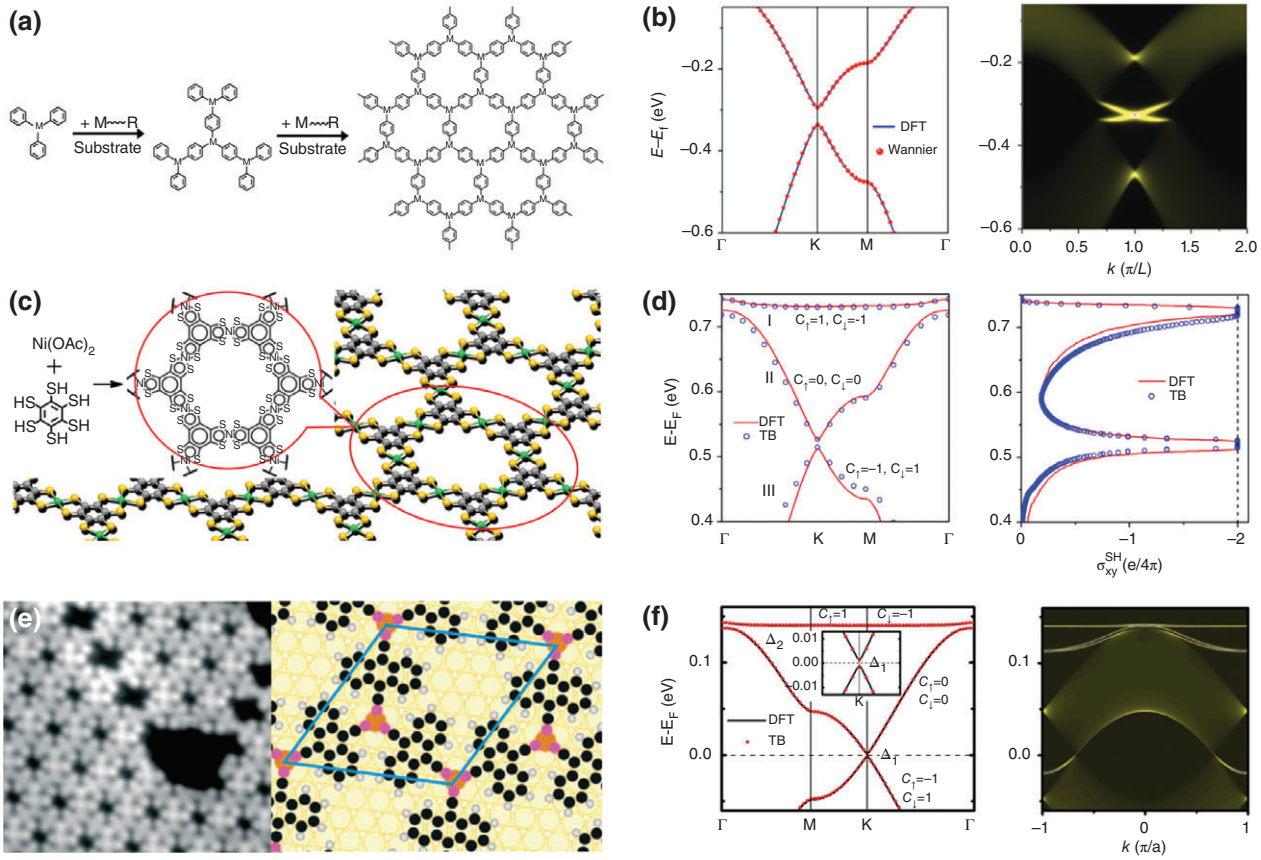

FIGURE 2 | (a) Schematic synthesis process from the triphenyl-metal molecules to the two-dimensional (2D) organometallic lattices. (b) Band structure and Dirac edge states of triphenyl-bismuth lattice with spin-orbit coupling (SOC). (Reprinted with permission from Ref 18. Copyright 2013 Nature Publishing Group) (c) Schematic illustration and chemical structure of monolayer nickel bis(dithiolene) complex nanosheet. (Reprinted with permission from Ref 61. Copyright 2013 American Chemical Society) (d) Kagome band structure for the flat and Dirac bands, and the quantized spin Hall conductance within the energy window of two SOC gaps. (Reprinted with permission from Ref 19. Copyright 2013 American Chemical Society) (e) Scanning tunneling microscope image of the hexagonal network of dicyanoanthracene on Cu(111) and the corresponding atomic model. (Reprinted with permission from Ref 62. Copyright 2013 Wiley) (f) Kagome band structure and Dirac edge states within two SOC gaps. (Reprinted with permission from Ref 20. Copyright 2016 American Chemical Society)

KM Model in Organometallic Framework

The first organic TI (OTI) was designed by applying the KM model to an organometallic framework made of triphenyl-bismuth molecule $Bi(C_6H_5)_3$.[18] It was proposed that a 2D 'organic' hexagonal lattice can be formed by assembling molecular building blocks of triphenyl-metal compounds, such as triphenyl-bismuth with strong SOC, as shown in Figure 2(a). There are two Bi atoms and three benzene rings with a chemical formula of $Bi_2C_{18}H_{12}$ in each unit cell and the neighboring benzene rings are bridge-bonded through the para-Bi atoms. The hexagonal lattice symmetry guarantees a Dirac band in such organometallic frameworks; while the heavy metal atom Bi, which is the most used component in topological materials, guarantees a large SOC. First-principles band structures shown a nontrivial SOC gap of ~43 meV at the Dirac point (Figure 2(b)). Nontrivial band topology was confirmed by both Z_2 invariant and edge state calculations. As for a typical KM model, a pair of topological edge states within the energy window of SOC gap is shown to connect the band edge between K and K′ and forming a 1D Dirac cone at the boundary of the Brillouin zone (Figure 2(b)). However, this system is not an intrinsic 2D OTI. To move its Fermi level into the SOC gap, two electrons per unit cell need to be removed. This can be achieved by either hole doping or design another lattice by substituting Bi with Pb with one less electron per atom.[18] Meanwhile, due to a larger unit cell and weaker SOC, the nontrivial SOC gap is reduced to ~8.6 meV when replacing Bi with Pb.

This initial work has since fostered a series of works in designing various 2D organic topological

materials.[47–56] For example, by simply replacing Bi with a transition metal atoms, such as Mn, a magnetic 2D OTI was designed to realize quantum anomalous Hall effect (QAHE), which can be explained by a spin-polarized version of KM model with an additional term of exchange field.[47] While replacing Bi with In, a topological flat-band material was designed to realize fractional QSH effect,[48] which can be explained by extending the two-band KM model to a four-band model.[57] If there is only one orbital per atomic site and nearest neighbor (NN) hopping in a hexagonal lattice, two Dirac bands arise. If there are two degenerate orbitals (p_x and p_y orbitals of In) per atomic site and NN hopping in a hexagonal lattice, four bands arise with two flat bands bracketing two Dirac bands. The SOC will open a nontrivial gap at the Dirac point as well as the two touching points between the flat and Dirac bands. Consequently, if the Fermi level lies inside the gap between the flat and Dirac bands, as the case of triphenyl-indium lattice, it results in a topological flat-band material. We refer the readers to a recent review[8] for detailed discussions of topological flat-band physics and materials.

π-Conjugated Framework of Kagome Lattice

It is very interesting to notice that in a typical organometallic framework made of metal atoms and phenyl rings as shown in Figure 2(a), the Bi atoms form a hexagonal lattice while the phenyl rings form a Kagome lattice. Conversely, if the metal atoms and phenyl rings switch their positions with each other, then the Bi atoms form a Kagome lattice while the benzene rings form a hexagonal lattice. Consequently, there will be two groups of bands arising from each sub lattice, namely Dirac bands and Kagome bands, in such π-conjugated frameworks. Specifically, the Kagome bands generally consist of one flat band and two Dirac bands.[19] In consideration of magnetism and SOC, it is well known that associated with its band structures, Kagome lattice is an ideal platform to study various exotic quantum phenomena, such as frustrated spin,[58] quantum spin liquid phase,[59] and fractional quantum Hall effect.[60]

Based on a bottom-up gas–liquid interfacial reaction approach, a single-layer π-conjugated nanosheet has been synthesized recently,[61] comprised of nickel bis(dithiolene) units with a chemical formula of $Ni_3C_{12}S_{12}$, as shown in Figure 2(c), which was recognized as a typical example of Kagome lattice made of Ni. There are three Ni atoms and three C_6S_6 rings in each unit cell. Its band structure is shown in Figure 2(d).[19] The SOC gap of the Dirac band is ~13.6 meV, and the SOC gap between the flat band and the top Dirac band is ~5.8 meV. Both gaps vanish in the absence of SOC as shown by first-principles calculations. The Chern number, used to characterize the nontrivial topology, is marked with different spin bands in Figure 2(d). For both spins, the flat band and the bottom Dirac band have a nonzero Chern number (± 1), while the top Dirac band has a zero Chern number. Thus, within both SOC gaps, the Chern number is zero but the spin Chern number is one, indicating that the $Ni_3C_{12}S_{12}$ lattice is a 2D OTI. The coexistence of two 2D TI states, one from the Dirac band and the other from a flat band, at different energies can be manifested in transport measurement. The spin Hall conductance as a function of energy has a quantized value ($-2e/4\pi$) within the energy window in both SOC gaps (Figure 2(d)). Similar to the hexagonal lattice made of triphenyl-Bi molecules, the Fermi level in this Kagome lattice is not in the SOC gap, and n-doping is needed. This requires doping two or four electrons, which corresponds to a doping concentration of $\sim 10^{13}$–10^{14} cm^{-2}. One can also replace Ni with Au atoms to increase the SOC. Overall, the band topology of the $Au_3C_{12}S_{12}$ lattice are the same as those of the $Ni_3C_{12}S_{12}$ lattice. The two SOC gaps are enhanced to ~22.7 and ~9.5 meV, respectively.

Intrinsic OTI of Cu-Dicyanoanthracene Framework

The distinct advantage of OTIs is their high tunability by using different metal atoms and molecular ligands. However, it is also important to note that as a coordination polymeric material, organometallic lattices are usually formed according to the specific electron counting rules of coordination chemistry. Consequently, substitution of the host metal atom with a foreign metal atom of different valence, which changes coordination chemistry, is usually difficult without changing the geometric structure. This is especially true for heavy doping up to the stoichiometric limit with all the host metal atoms replaced. Alternatively, doping of organometallic lattices may be achieved by changing the oxidation states of the metal ions through redox control.[49] However, such a process is still limited by the amount of doping it can achieve. Therefore, it is highly desirable to design intrinsic 2D OTIs without doping.

Recently, a Kagome lattice made of Cu-dicyanoanthracene (DCA) has been synthesized experimentally on Cu(111) substrate,[62] as shown in Figure 2(e). Each Cu atom bonds with three CN

groups from the DCA molecules to form a strong coordination bond. There are two Cu atoms and three DCA molecules in each unit cell, which has a hexagonal lattice formed by Cu atoms and a Kagome lattice formed by DCA molecules. The calculated topological band structures and edge states are similar to those of $Ni_3C_{12}S_{12}$ lattice, but the Fermi level lies inside the Dirac SOC gap (~2.9 meV),[20] as shown in Figure 2(f). Such intrinsic TI states are found to originate from a proper number of electrons filling the hybridized bands from Cu atomic and DCA molecular orbitals. Furthermore, substituting Cu with Au atom will increase the SOC gap to ~11.3 meV, but without changing the Fermi level.

SURFACE-BASED 2D TOPOLOGICAL MATERIALS

So far, most theoretically designed 2D topological materials are freestanding films. However, the existence of many proposed 2D freestanding films could be in doubt because of their poor thermal or chemical stability. Even if they do exist, the growth and synthesis of freestanding films are usually harder than growth of thin films on a substrate. In addition, when a topological freestanding film is transferred on a substrate, which is often required for measurements or building a device, its topological properties may be altered or lost due to its inevitable interaction with the substrate. One known example is the freestanding Bi(111) bilayer film, which is a large gap 2D TI.[63–66] However, when it is grown on Bi_2Se_3 and Bi_2Te_3 substrates,[36,67,68] it shows metallic features with a hybridized band structure resulting from a strong interfacial interaction, as indicated by angle-resolved photoemission spectroscopy (ARPES) measurements. Although topological edge states have been revealed by STS measurement in real space,[36–38] more direct evidence of quantized conductance would be difficult to obtain by transport experiments. To overcome this difficulty, a new concept of surface-based 2D topological materials has recently been proposed[21] through computational design of growth of a metal overlayer on a semiconductor substrate that exhibits topological surface states,[21–23,69–80] which are benign to interfacial interactions.

Substrate Atomic Orbital Filtering Effect

We briefly review the key working mechanism that underlies the surface-based 2D topological materials, the substrate atomic orbital filtering effect. It makes the metal overlayer atomically bonded to but electronically isolated from the underlying substrate.[21] To illustrate the importance of three designing ingredients of lattice symmetry, SOC and atomic orbital composition, a 'computational experiment' was conducted[21] on two artificial 'graphene' made of Bi and Au instead of C, which presumably have a much larger SOC than C. Surprisingly, it was found that the planar Bi lattice has $Z_2 = 0$, while the Au lattice has $Z_2 = 1$. More generally, one can better understand the topological phases in a 2D hexagonal lattice by a multi-orbital tight-binding model beyond the original KM model. Then the Bi lattice can be described by the p-orbital six-band model. Owing to the planar symmetry, p_x and p_y oribitals hybridize to be distinguished from the p_z orbital, resulting in two branches of energy bands. The p_z branch of π and π^* bands is exactly the same as graphene. The (p_x, p_y) branch has four bands: two flat bands bracketing two Dirac bands, as described by the four-band model mentioned above.[57] It is well known that these two branches of bands are both topologically nontrivial separately; however, together they become trivial as the sum of two odd topological invariant becomes even. On the other hand, the planar Au lattice can be described by the s-orbital two-band model, in an analogy to graphene. Without SOC, the two s orbitals hybridize into linearly dispersive two-fold degenerate σ and σ^* bands which touches at K point (Dirac point); the SOC opens a gap and mixes the σ and σ^* bands into two sets of $\sigma \pm i\sigma^*$ bands encoding a nontrivial topology.

There are two ways to make the planar hexagonal Bi lattice topologically nontrivial. The first way is by the well-known band inversion approach,[10] which in the present case can be achieved by buckling the lattice into a non-planar structure (Figure 3(a)), i.e., the single Bi(111) bilayer. Figure 3(b) shows the band structure and density of states (DOS) of a Bi(111) bilayer, which is confirmed with nontrivial topology.[21] In such a buckled structure, the Bi—Bi bond angle is around 90°, indicating that three (p_x, p_y, and p_z) orbitals are degenerate with each other. Chemical bonding and crystal field splitting lift the degeneracy and forms one set of doubly degenerate $\sigma_{1,2}$ and $\sigma_{1,2}$* bands and another set of non-degenerate σ_3 and σ_3* bands, in the order of energy as shown in Figure 3(c). The SOC opens an energy gap and further lifts the degeneracy of $\sigma_{1,2}$ and $\sigma_{1,2}$* bands, as well as causes a band inversion of energy order between $\sigma_{1\pm i2}$ and σ_3* bands around the Fermi level. Consequently, the overall band topology becomes nontrivial.

The second approach is to simply remove one branch of orbitals [either (p_x, p_y) or p_z] to reduce the trivial six-band lattice into a nontrivial two- or four-

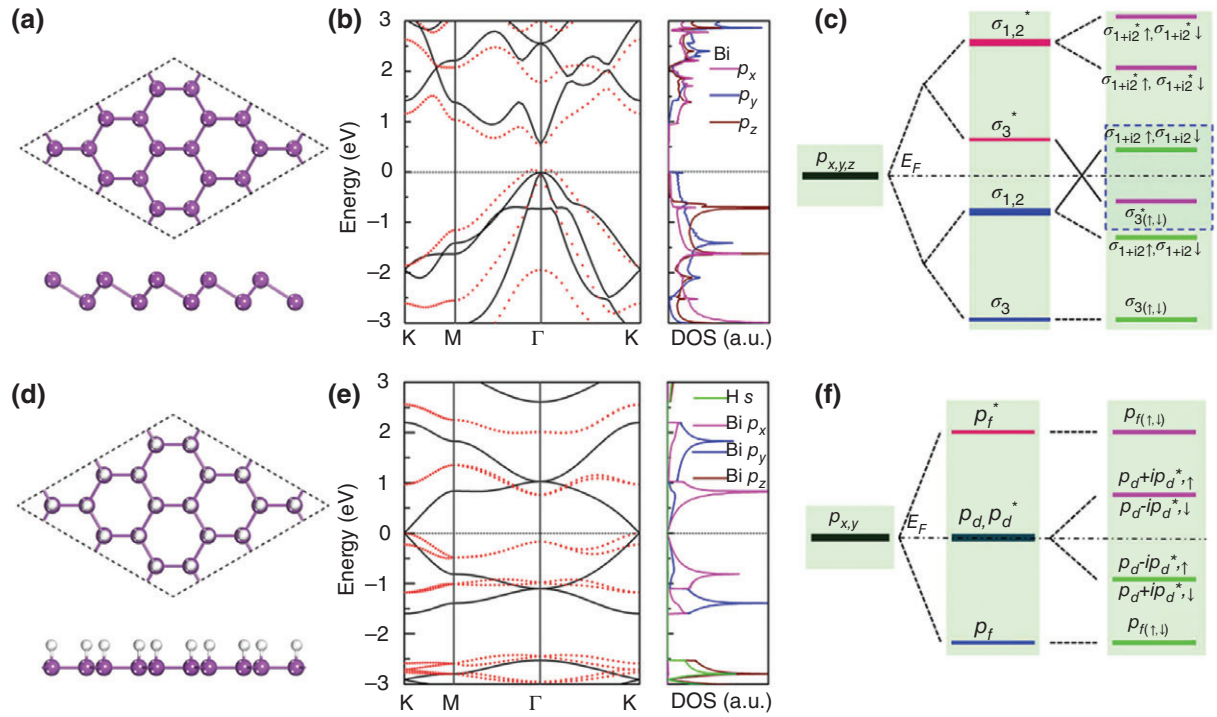

FIGURE 3 | (a)–(c) Structural model, band structure and atomic-orbital projected density of states (DOS), and the energy diagram (at Γ point), respectively, of a buckled Bi(111) bilayer. The band inversion is highlighted by a dashed rectangle. (d)–(f) Same as (a)–(c) for planar Bi hexagonal lattice with one side saturated by H. (Reprinted with permission from Ref 21. Copyright 2014 National Academy of Sciences)

band lattice. To verify this idea, one may artificially saturate the planar hexagonal Bi lattice with H to remove the p_z orbital (Figure 3(d)).[21] It was found that the p_z orbital of Bi hybridizes strongly with s orbital of H, shifting away from the Fermi level, so that the system reduces to a (p_x, p_y)-orbital four-band model, which supports a nontrivial topological phase (Figure 3(e) and (f)). Of course, the clean or hydrogenated planar hexagonal Bi lattice is artificial, does not exist; but the revealed physical mechanism of 'H orbital filtering effect' can be employed by growth of Bi overlayer on a substrate through a 'substrate orbital filtering effect,' where the substrate surface atoms will play the role of H atoms to remove the p_z orbital of Bi, as demonstrated below using the example of growth of Bi on halogenated Si(111) surface.

Bi-Cl/Si(111) Surface

As the basic material used in the semiconductor industry, the surface of Si has been extensively studied. At low temperatures, the Si(111) surface has a complex reconstructed structure, as the reconstruction eliminates the dangling bonds and reduces surface energy. However, at high temperature, the Si(111) surface can retain an unreconstructed structure with one dangling bond on each surface atom. Owing to the strong steric repulsion between the halogen atoms, a superlattice structure can be formed on Si(111) surface at 1/3 monolayer (ML) halogen coverage, which was reported in X-ray standing-wave experiments long time ago.[81] Most importantly, the unsaturated two dangling bonds provide a natural hexagonal template to guide the epitaxial growth of metal atoms, hence driving the metal atoms to form a hexagonal lattice,[21] as shown in Figure 4(a). Moreover, a large energy barrier is present for metals to diffuse out of the template. For example, an energy barrier of 4.9 eV must be overcome for Bi to jump from Si to neighboring Bi sites, indicating high thermodynamic and kinetic stability of the designed 2D hexagonal metal lattice.

The band structures of Bi-Cl/Si(111) surface was analyzed by the first-principles calculations.[21] Without SOC, there are two Dirac band residing inside the bulk gap of Si with a Dirac point at K point for Bi-Cl/Si(111), as shown in Figure 4(c). Band composition analysis further showed that the two Dirac bands are mainly constructed from p_x and p_y orbitals of Bi, as shown in Figure 4(b). The p_z orbital of Bi hybridized strongly with the dangling bond of surface Si atom and hence is moved away from the

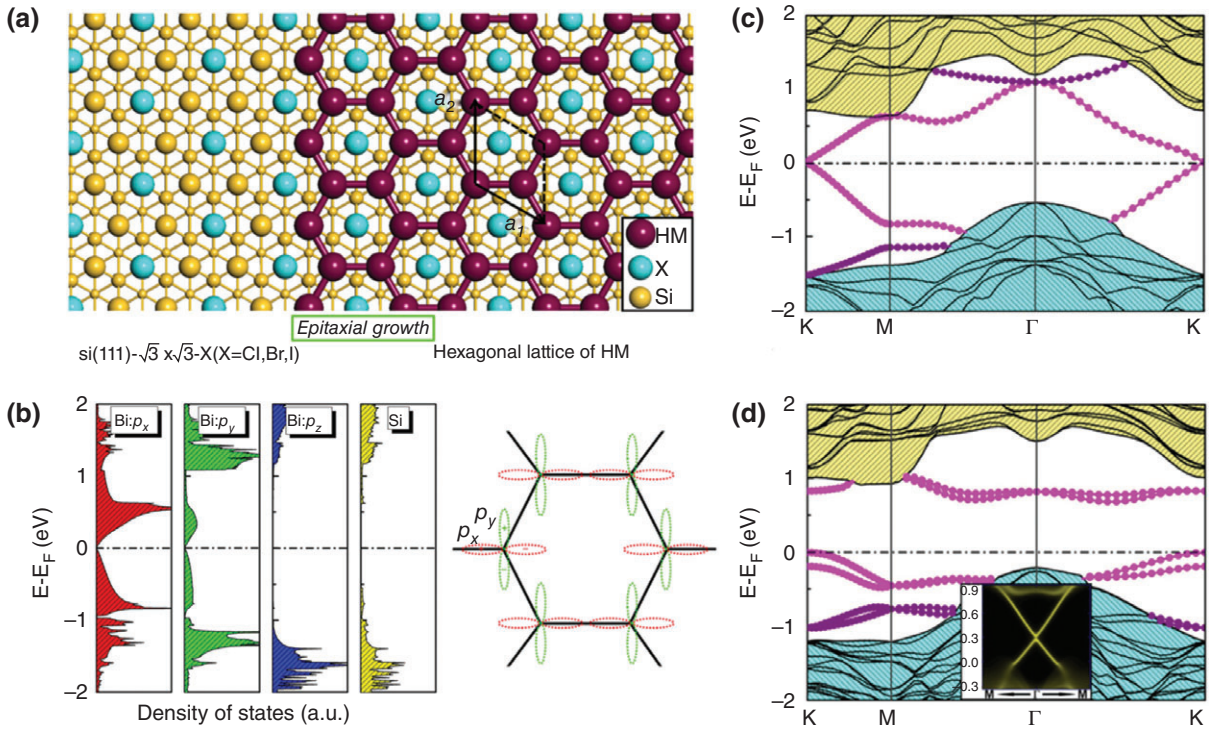

FIGURE 4 | (a) Schematic epitaxial growth of heavy metal (HM) atoms on the 1/3 halogen covered Si(111) substrate, forming a hexagonal lattice made of HM atoms. (b) The projected density of states (DOS) and schematic hexagonal lattice made of p_x and p_y two orbitals on each site. (c) and (d) Band structures of Bi on Si(111)-$\sqrt{3}\times\sqrt{3}$-Cl [Bi-Cl/Si(111)] surface without and with spin-orbit coupling (SOC). Inset shows the Dirac edge states within the SOC gap of Bi-Cl/Si(111). (Reprinted with permission from Ref 21. Copyright 2014 National Academy of Sciences)

Fermi level to leave only the p_x and p_y orbitals. Additionally, there are two weakly dispersive bands, consisting of also p_x and p_y orbital of Bi, siting one below and the other above the Dirac band and touching the Dirac band at Γ point. Such a band structure is very similar to the four-band model in a hexagonal lattice with p_x and p_y orbitals at each lattice site,[57] as shown in Figure 4(b). By including the SOC (Figure 4(d)), the two Dirac bands are split apart and a large energy gap of ~0.78 eV is opened at K point. Considerable energy gaps are also opened by SOC between the weakly dispersive band and Dirac band at Γ point. Owing to the inversion symmetry breaking induced Rashba effect, the spin band degeneracy is also lifted. The nontrivial topology of the Bi-Cl/Si(111) is characterized by the topological edge state calculations, as shown in the inset of Figure 4(d). A pair of gapless edge states connecting the upper and lower bulk band edge to form a 1D Dirac cone at the center of Brillouin zone, demonstrating a 2D TI phase. Here, the Cl/Si(111) substrate performed as an orbital filter, to selectively remove the p_z orbitals from the Bi lattice, reducing it from a trivial six-band lattice to a nontrivial four-band lattice. Therefore, the Bi overlayer is atomically bonded but electronically isolated from the underneath semiconductor substrate. The above physics is general, it is also applicable to different metal atoms. For example, Bi atoms can be substituted with other heavy metal atoms, such as Pb, Sb, Sn, Ga, In, and Tl on hydrogenated Si(111) surface.[69] Similar topological states can be observed, but with a tunable size of SOC gap. Also, using a transition metal atom, such as W, a surface-based magnetic 2D TI forms leading to QAHE.[70] Similarly, the same approach can be extended to using different substrates, such as Ge[80]and SiC[72] substrates.

Minimal-Basis QSH Model in Trigonal Lattice

To enhance SOC, naturally heavy metal atoms are preferred. However, usually metal atoms favor a close-packing geometry forming trigonal lattice in 2D rather than the open hexagonal and square lattice, as employed originally in the KM and BHZ model, respectively. In fact, many heavy metal atoms grown on a semiconductor surface have been found to exhibit a trigonal lattice symmetry.[82–84] For this reason, a minimal-basis QSH lattice model

consisting of three orbitals (s, p_x, p_y) in a trigonal lattice was introduced recently.[22] These three basis orbitals, as shown in Figure 5(a), can be equivalently transformed into three sp^2 hybridized orbitals, as shown in Figure 5(b). It has been shown that depending on the order of energy of s versus p orbital (E_s vs E_p), there are two different types of bands.

In the first type, the s-band is above the p-band ($E_s > E_p$) without SOC, as shown in Figure 5(c). The red and blue colors indicate the components of s and p orbital, respectively, and the parities for each sub-band at TRIM[24] (Γ point and three M points) are labeled with + and – sign. It is found that the topological invariant is $Z_2 = 0$ for middle and bottom two sub-bands, indicating clearly a normal insulator (NI) phase. In order to realize the QSH phase, an SOC induced s–p band inversion is needed ($E_s < E_p^{\lambda}$), i.e., first closing of a trivial gap followed by reopening of a nontrivial gap by including the SOC. With the increasing SOC strength, one can see that the band gap between top and middle sub-band first reduces and closes (Figure 5(d)), and then reopens (Figure 5(e)) at the Γ point. The s–p band inversion induces a parity exchange in this process, so that the topological invariant changes from $Z_2 = 0$ (Figure 5(c)) to $Z_2 = 1$ (Figure 5(e)) for the middle and bottom two sub-bands.

In the second type, the s-band is below the p-band ($E_s < E_p$) without SOC, as shown in Figure 5(f). Different from Figure 5(c), the topological invariant is already $Z_2 = 1$ for the middle and bottom two sub-bands, i.e., the band order has already been inverted even without SOC. Thus, any finite SOC will open a

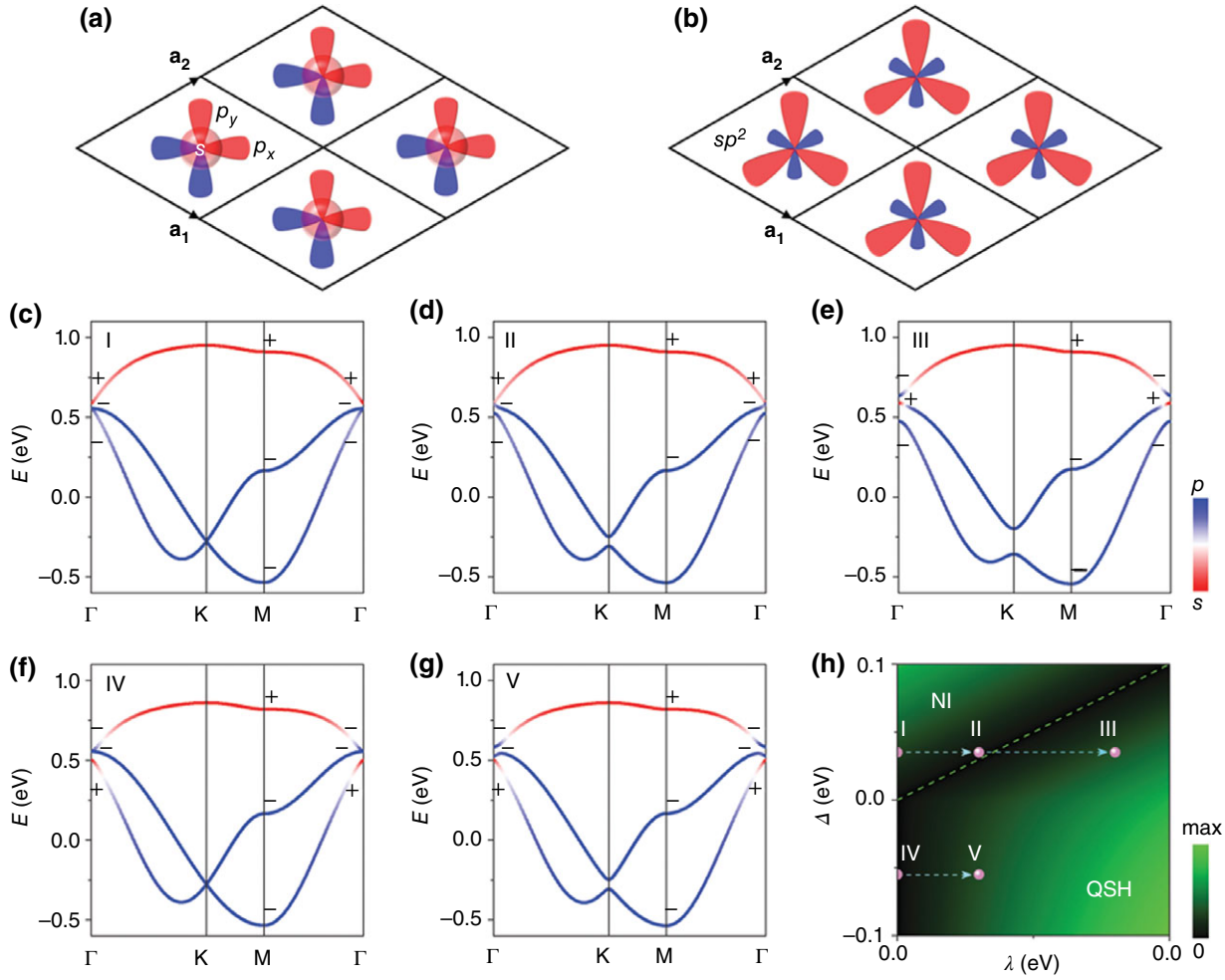

FIGURE 5 | (a) and (b) Trigonal lattice with three orbitals (s, p_x, p_y) per lattice site and its equivalent three sp^2 orbitals. (c)–(e) The first-type band structures with the increasing spin-orbit coupling (SOC) strength. (f) and (g) The second-type band structures without and with SOC. (h) Topological phase diagram in the parameter space, showing normal insulator (NI) and quantum spin Hall (QSH) phases. (Reprinted with permission from Ref 22. Copyright 2016 Nature Publishing Group)

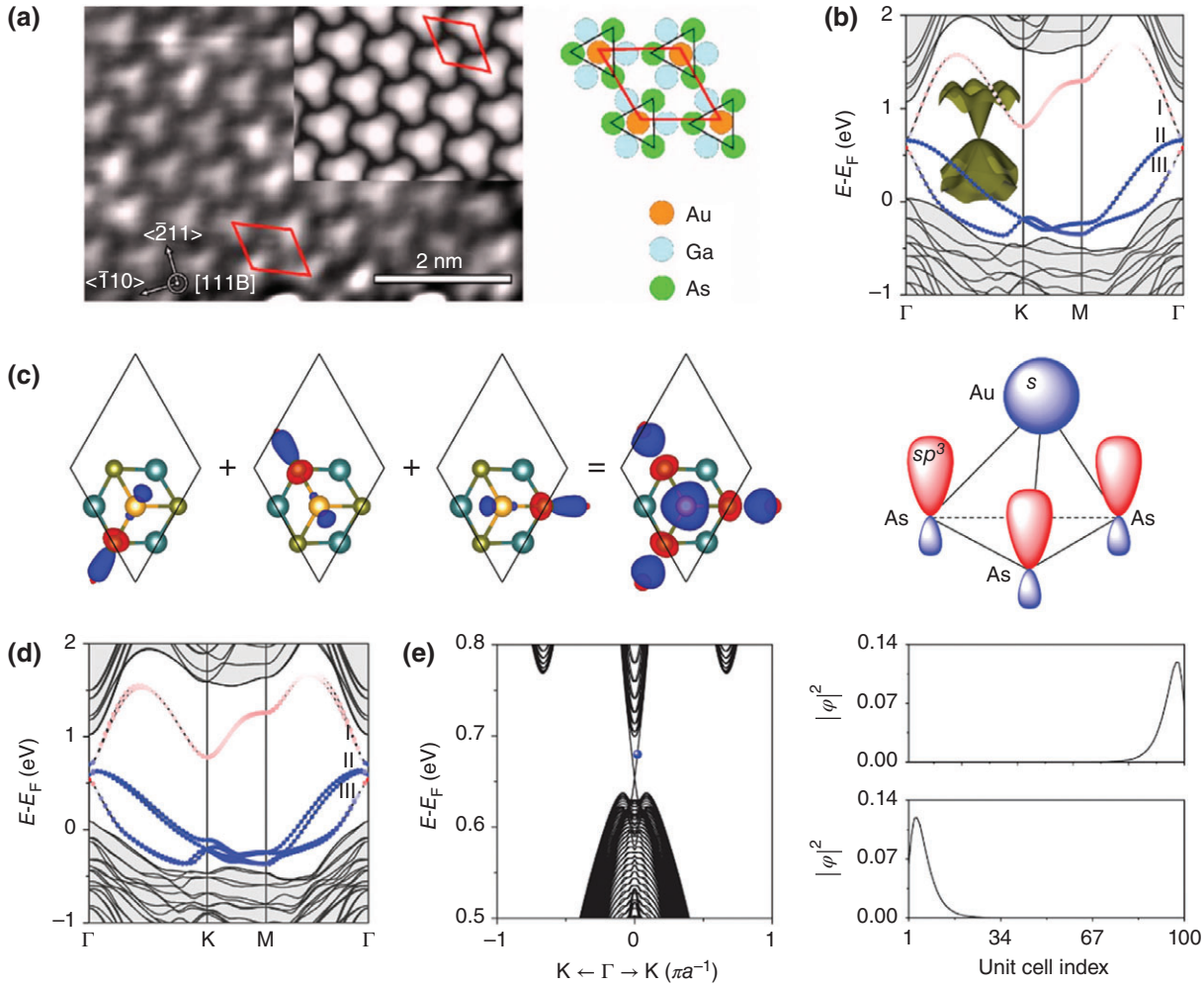

FIGURE 6 | (a) Experimental and simulated scanning tunneling microscope images for Au grown on GaAs(111) surface, forming a trigonal lattice. (Reprinted with permission from Ref 84. Copyright 2006 American Institute of Physics) (b) Band structures of Au/GaAs(111) without spin-orbit coupling (SOC). The inset is a 3D band plotting of the Dirac band. (c) Three fitted Wannier orbitals and the corresponding schematic un-hybridized surface orbitals. (d) Band structures of Au/GaAs(111) with SOC. (e) 1D topological edges states and their real space distributions. (Reprinted with permission from Ref 22. Copyright 2016 Nature Publishing Group)

nontrivial gap at Dirac point to turn the system into a QSH phase similar to KM model,[9] as shown in Figure 5(g). This second type of QSH phase in a trigonal lattice has also been recently discussed with multiple p-bands in a $k \cdot p$ model.[75] The parity does not change by including the SOC in this process. Based on the above band order analysis, a topological phase diagram can be constructed, as shown in Figure 5(h). Using $\Delta = E_s - E_p$ and the SOC parameter λ as two independent parameters, NI and QSH phase is divided by the band gap closing line [$E_s = E_p^{+\lambda}$, dashed line in Figure 5(h)]. The parameters used for band structure in Figure 5(c)–(g) are labeled with I–V. We have marked these data points in the phase diagram (Figure 5(h)), with dashed arrows indicating the increasing SOC strength to distinguish these two different QSH phase realization processes.

Au/GaAs(111) Surface

Interestingly, the above minimal-basis QSH model has been found to be exactly realizable in Au/GaAs(111) surface. At low coverage of Au on the As-terminated GaAs(111)B surface, a $\sqrt{3}\times\sqrt{3}$ trigonal superlattice structure is observed experimentally,[84] as shown in Figure 6(a). Also, a theoretical model with one Au atom adsorbed on every third hexagonal close-packed (hcp) threefold hollow site of the Ga lattice is shown to be the most energetically stable, with a simulated STM image in

excellent agreement with the experiment (Figure 6 (a)). Starting from the experimental structure of Au/GaAs(111), its first-principles band structure without SOC is shown in Figure 6(b).[22] There is a Dirac cone at the Γ point above the Fermi level, which are well separated from the other bulk bands (shaded region). The highlighted three bands can be well reproduced by the Wannier fitting. The fitted three Wannier orbitals are shown in Figure 6(c), which are equivalent to each other and have mixed components from both As-p and Au-s orbitals. Adding them together, the overall orbital shape is an s-type orbital centered at Au atom, and three tilted p-type orbitals centered at three surface As atoms along the As-Au bond direction. This forms effectively a sp^2 hybridization, which is comparable to the un-hybridized surface orbitals of Au and As atoms, as schematically shown in Figure 6(c) and satisfies perfectly the conditions for the minimum basis model of three orbitals (s, p_x, and p_y) in a trigonal lattice described above. The band structure of Au/GaAs (111) with SOC is shown in Figure 6(d), and an SOC gap of ~73 meV is opened at the Γ point, which facilitates possibly the room-temperature measurement. In addition, the inversion symmetry is broken in Au/GaAs(111), so that the band degeneracy is lifted by Rashba splitting. 1D ribbon band structure of Au/GaAs(111) is shown in Figure 6(e). A pair of gapless edge states with a Dirac cone at the Γ point, which are energy-degenerate for opposite edges, are seen within the SOC gap. The real space distribution of the edge states, at the energy marked by blue dot in the band structure, is shown in Figure 6(e). Clearly, the degenerated edge states are spatially localized at the opposite edges of the ribbon, directly confirming Au/GaAs(111) to be a 2D TI. However, the Fermi level of Au/GaAs(111) is not in the SOC gap, so n-doping is needed. Alkali-metal atoms have been widely used for surface n-doping in the experiments, including graphene,[85] superconducting FeSe[86] and metal film.[82] At 5/12 monolayer coverage of alkali-metal atoms, the Fermi level of Au/GaAs(111) can be tuned into the SOC gap without affecting the bands of host system.[22]

FeSe/$SrTiO_3$(001) Film

In the above-mentioned surface-based 2D topological materials, there exists a strong interfacial interaction between the metal overlayer and substrate. On the other hand, if the interfacial interaction is weak such as of van der Waals type, then the topological properties of the overlayer, if exists, is expected to be retained on the substrate. In this case, one simply needs to identify and design the overlayer to be topologically nontrivial. One such example is the recent discovery of a 2D TI in single-layer FeSe grown on $SrTiO_3$(001) (STO) substrate.[23] Superconducting and topological states are two most intriguing quantum phenomena in solid materials. The entanglement of these two states, the topological superconducting state, will give rise to even more exotic quantum phenomena. While many materials are found to be either a superconductor or a TI, this is the first time that these two exotic phases are found to coexist in one single 2D material.

The single-layer FeSe/STO film has drawn much recent attention as a high-temperature 2D interfacial superconductor, and the underlying physical mechanism is still under debate. Interestingly, possible existence of topological phases in the square lattice of superconductor FeSe has also been suggested.[87–90] In the superconducting phase, the Fermi surface of FeSe/STO is characterized with electron pockets at M point but no hole pockets at Γ point, and there is also an energy gap of ~40 meV below the Fermi level at M point.[91–93] However, these key features have not been well understood theoretically. To solve this problem, an indirect approach was taken to match the experimental ARPES with the calculated band structure of FeSe/STO in non-magnetic and different possible magnetic configurations.[23] It was found that the band structure of FeSe/STO with checkerboard antiferromagnetic (AFM) configuration (Figure 7(a)) can match the ARPES spectra best, not only around Γ and M point but also within the whole Brillouin zone. Most remarkably, by including the SOC, an energy gap of ~33 meV (absence without the SOC) is opened at the M point below Fermi level, in good agreement with the ARPES spectra, as shown in Figure 7(d).

Generally, the band gap opened by SOC is topological nontrivial. To characterize this, 1D edge states of FeSe/STO ribbon with both ferromagnetic (FM) and AFM edges were calculated, as shown in Figure 7(e). For FM edge, there are two asymmetric edge states inside the SOC gap for both left and right edges, and the Dirac point is not at high symmetry k point. For AFM edge, the edge states become symmetric, and the Dirac points are at high symmetry k point. Inside the SOC gap, the valence and conduction bulk bands are connected with a pair of gapless Dirac edge state for both FM and AFM edges, demonstrating the characteristic feature of AFM topological states, which is consistent with theoretical prediction in HgTe quantum well with a magnetic stagger potential.[94]

Furthermore, to confirm the AFM topological edge states in FeSe/STO, the STS measurement were

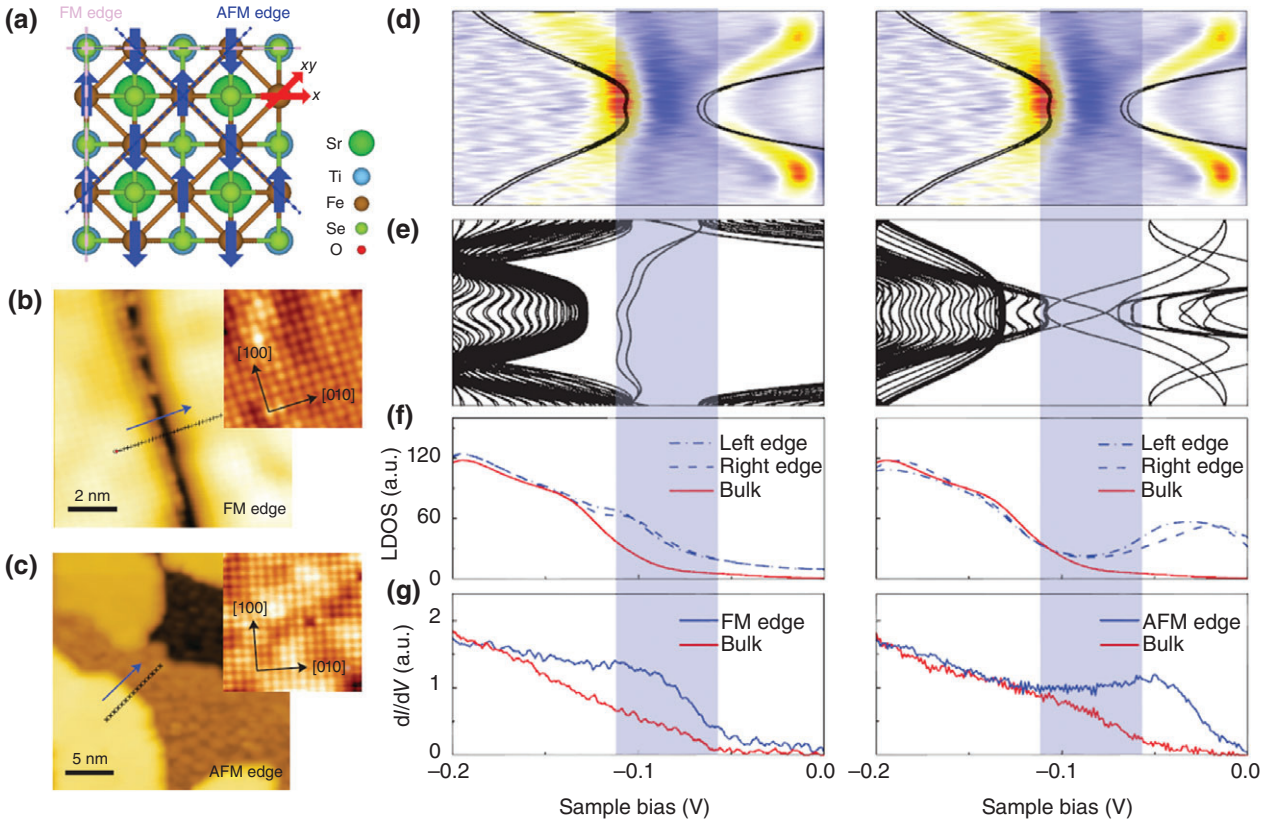

FIGURE 7 | (a) Top view of FeSe/STO, with a checkerboard antiferromagnetic (AFM) spin configuration on Fe atoms. (b) and (c) Scanning tunneling microscope (STM) images for FM edge and AFM edge of FeSe/STO. The inset shows an atomic-resolution STM image at the bulk position, showing the topmost Se atom arrangement. (d) Theoretical and angle-resolved photoemission spectroscopy (ARPES) band structure around the M point. (e) 1D band structure of a FeSe/STO ribbon with FM and AFM edges. (f) Local density of states (LDOS) for edge and bulk states. (g) Scanning tunneling spectroscopy (STS) spectra of edge and bulk states for FM and AFM edges. The light blue band indicates the spin-orbit coupling (SOC) gap. (Reprinted with permission from Ref 23. Copyright 2016 Nature Publishing Group)

taken along both FM and AFM edges of FeSe/STO, as shown in Figure 7(b) and (c), respectively. By setting the Fermi level as the reference energy, ARPES and theoretical bands around the M point (Figure 7(d)), 1D bands for FM and AFM edge (Figure 7(e)), LDOS for FM edge and AFM edge (Figure 7(f)) are aligned with the STS spectra for FM edge and AFM edge (Figure 7(g)), with the region of the SOC gap indicated by the light blue band. Clearly, the STS spectra of FM and AFM edges have a larger intensity in the expect energy window of SOC gap. Importantly, the shape and overall tendency of STS spectra of both FM and AFM edges versus bulk can be qualitatively reproduced by theoretical LDOS. For FM and AFM edges, the maximum difference between the calculated edge and bulk DOS is within and above the SOC gap, which is also observable in the experimental STS spectra. Thus, the STS spectra provided strong evidence to confirm the existence of topological edge states in FeSe/STO. This finding affords an exciting opportunity to study 2D topological superconductors through the proximity effect by interfacing a superconductor with a TI through a p-n junction, since n- and p-type FeSe is respectively a superconductor and TI.

TRANSITION METAL ATOMS-BASED QSH INSULATOR: d-ORBITAL INVOLVED BAND INVERSION

As discussed above, the emergence of the nontrivial phase can be achieved by the band inversion with the parity exchanged. The conventional band inversion mechanism typically involves s–p band inversion. In designing topological materials, other orbital can also be involved in the band inversion process, particularly the d-orbital involved in the d–p or d–d type of band inversion. This naturally extend the topological materials to transition metal elements with d-orbital valences and to magnetic topological materials, such as the magnetic 2D OTI with Mn[47] and surface-

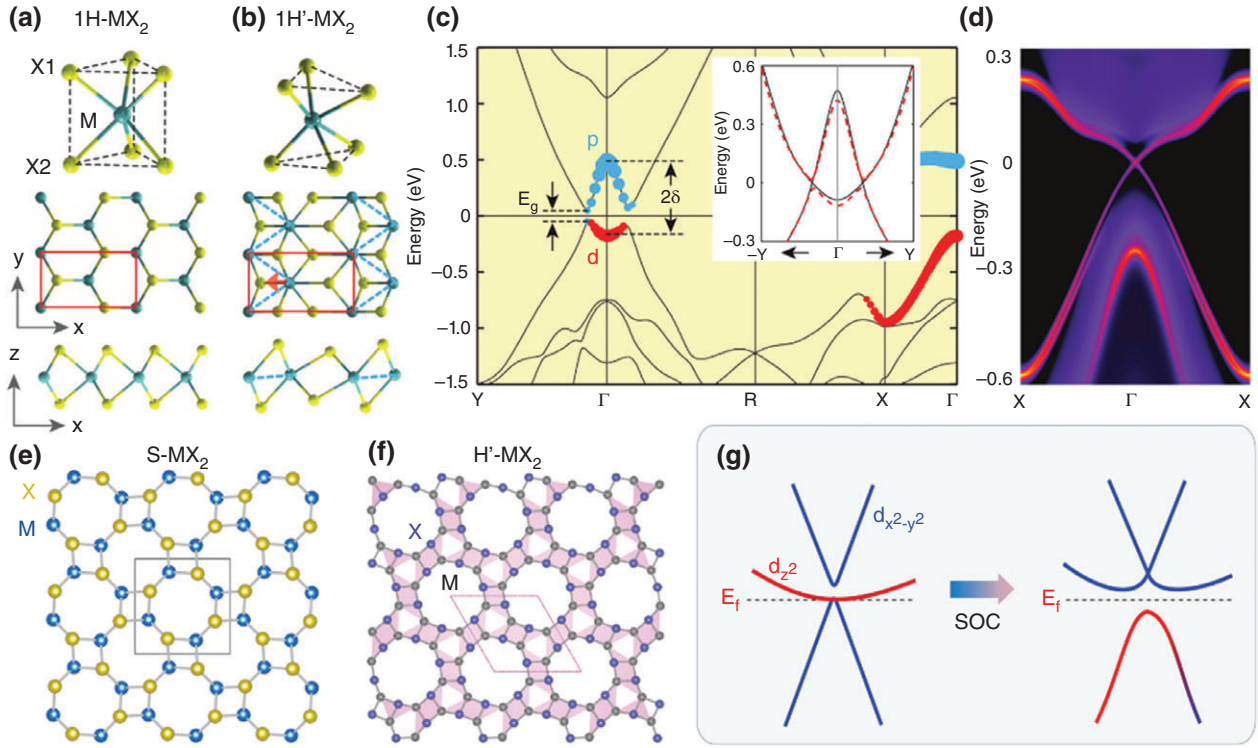

FIGURE 8 | Atomistic structures of monolayer transition metal dichalcogenides (TMDCs) for (a) 1H-MX_2 and (b) 1T′-MX_2. (c) Band structure of 1T′-MoS_2. E_g is band gap; 2δ is inverted gap. The inset compares band structures with (red dashed line) and without (black solid line) spin-orbit coupling (SOC). (d) Calculated edge states at Γ point. (Reprinted with permission from Ref 96. Copyright 2014 American Association for the Advancement of Science) (e) Atomic configuration of (e) square MX_2 (S-MX_2) and (f) hexagonal MX_2 (H′-MX_2). (g) The evolution of orbital-resolved band structures of 1S-MoS_2 near Γ point when considering SOC. The low energy bands near the Fermi level (E_f) are mainly contributed from the d_{z^2} and $d_{x^2+y^2}$ orbitals of transition metal. (Reprinted with permission from Refs 100 and 102. Copyright 2015 American Physical Society)

based magnetic 2D TI with W on halogenated Si surface[70] for QAHE we briefly mentioned above, as well as the AFM QSH phase in monolayer FeSe we discussed in detail. In addition, there are at least two other classes of 2D TIs involving d orbitals which have been studied extensively.

Transition Metal Dichalcogenides

Recently, among all the predicted and synthesized 2D crystals, transition metal dichalcogenides (TMDCs) MX_2 with M = (Mo, W) and X = (S, Se, Te), are particularly appealing because of their unique physical properties and potential applications in various electronic and optical devices.[95] Using first-principles calculations, Qian et al.[96] predict a class of QSH insulator in TMDCs with 1T′ structure, namely, 1T′-MX_2, although most of TMDCs with 1H structure are not 2D TIs. Figure 8(a) and (b) shows the structures of MX_2 including the 1H and 1T′ phases. A structural distortion to 1T′ phase causes the band inversion and thereby leads to the topological phase transition from trivial to nontrivial. Figure 8(c) shows a typical band structure of 1T′-MoS_2. Near Γ point, the conduction and valence bands display a 'W' and 'M' shape, suggestive of band inversion with a gap of 0.08 eV. Analyzing the orbital character, the valence band mainly consists of metal d orbitals and the conduction band mainly consists of chalcogenide-p orbitals. This d–p band inversion is responsible for the nontrivial band topology.[96–98] The QSH insulator in 1T′-MX_2 leads to helical edge states that are protected from localization and backscattering by TRS (Figure 8(d)). Monolayer MX_2 may exhibit other structural phases. Interestingly, it was predicted recently that the square phase (S-MX_2)[99–101] and the hexagonal phase (H′-MX_2)[102] are 2D TI based on DFT calculations (Figure 8(e) and (f)). These phases can be expected to be prepared experimentally and have relatively sizeable band gaps. Different form QSH in the 1T′ phase where the inversion bands are mainly from the p and d orbitals, the inversion orbitals of the 1S phase are dominated by the d orbitals (Figure 8(g)).

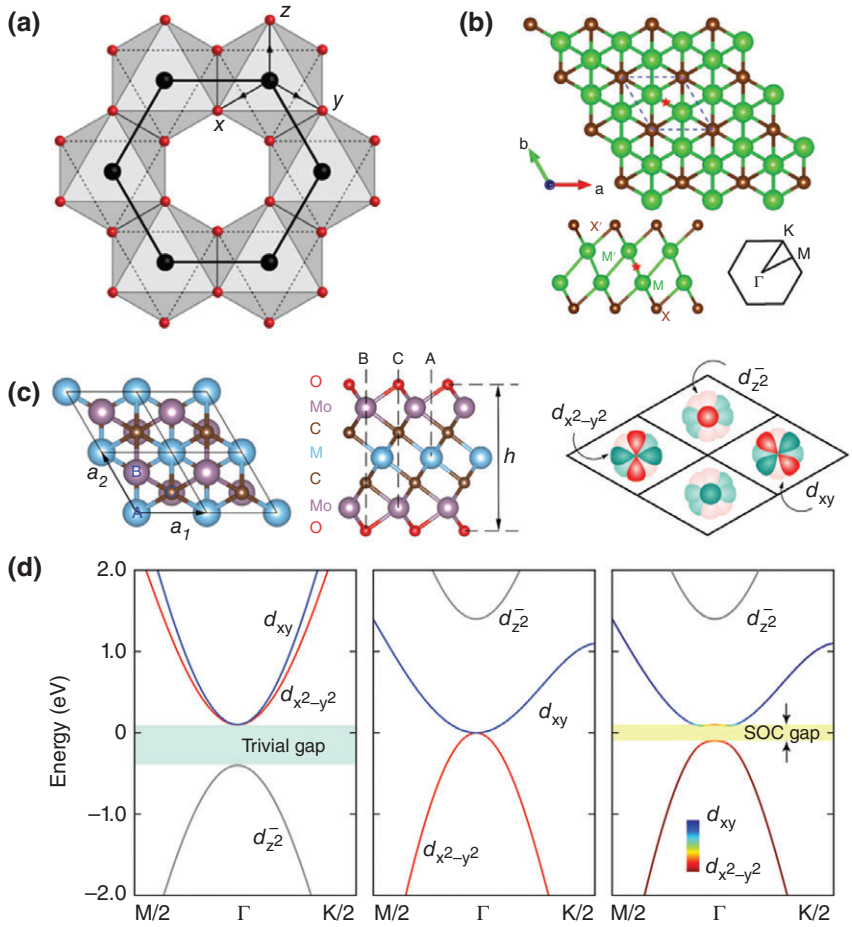

FIGURE 9 | (a) The honeycomb lattice of Ir atoms in Na_2IrO_3. A large black circle shows an Ir atom surrounded by six O atoms (red small circles). (Reprinted with permission from Ref 103. Copyright 2009 American Physical Society) (b) The top and side view of MX monolayer, respectively. (Reprinted with permission from Ref 104. Copyright 2015 American Chemical Society) (c) The top (left) and side (middle) view of the crystal structure of Mo_2MC_2 (M = Ti, Zr, or Hf) MXene displaying the hexagonal unit cell with lattice vector a_1 and a_2. Trigonal lattice with three d (d_{z^2}, d_{xy}, $d_{x^2-y^2}$) orbitals per lattice site (right). (d) Evolution of band structure of trigonal lattice with d orbitals. Normal band order, left; inverted band order without spin-orbit coupling (SOC), middle; inverted band order with SOC gap, right. (Reprinted with permission from Ref 106. Copyright 2016 American Chemical Society)

Transition Metal Oxides/Halide/Carbides

Shitade et al. proposed a way to design TIs in 5d transition metal oxides based on first-principles calculations.[103] A newly synthesized compound Na_2IrO_3 (Figure 9(a)) is predicted to be a QSH insulator, in which 5d orbital plays crucial roles in the nontrivial phase. Also, transition metal halide, MX (M = Zr, Hf; X = Cl, Br, and I) monolayers are proposed as QSH insulator.[104] MX monolayer has the simplest stoichiometric ratio and its interlayer binding energy is comparable to other layered systems (Figure 9(b)). A novel MX family shows large tunable nontrivial gaps in the range of 0.12–0.4 eV. The origin for the QSH effect is from the band inversion between transition metal (d_{xy}, d_{xz}) orbitals and (d_{xy}, $d_{x^2-y^2}$) orbitals. Moreover, the functionalized transition metal carbides known as MXenes M_2CO_2 (M = W, Mo, and Cr)[105] and $Mo_2MC_2O_2$ (M = Ti, Zr, and Hf)[106] are predicted as robust QSH insulators. Especially, a new class of MXenes which contain double transition metal elements in a fully ordered structure, such as Mo_2TiC_2 and Cr_2TiC_2, have been synthesized. First-principle calculations of band structures, Z_2 topological invariants and edge states as well as a TB model based on the d_{z^2}-, d_{xy}-, and $d_{x^2-y^2}$ -orbital basis in a triangular lattice are used to reveal the nontrivial topological properties of $Mo_2MC_2O_2$ (Figure 9(c) and (d)). There are three important advantages for the QSH states discovered in $Mo_2MC_2O_2$. First, the topological orders in MXenes represent a new class of d-band QSH phase in a triangular lattice (Figure 9(d)), which extends the

search of QSH insulators from honeycomb and square lattices to triangular lattices and hence will greatly broaden the scope of topological materials. Second, the atomic SOC strength of M totally contributes to the topological gap at the γ point, which gives rise to sizeable bulk gaps from 0.1 to 0.2 eV for $Mo_2MC_2O_2$ depending on the choice of M atoms. In contrast, the topological gap is much smaller than the atomic SOC strength in those systems predicted based on the classic KM or BHZ model. Third, MXenes are usually fabricated by immersing MAX powers in acidic solutions, so the surfaces of MXenes are inevitably terminated by primarily O and/or OH groups, and the latter can be converted into O termination by high temperature annealing or by metal adsorption. Thus, the $Mo_2MC_2O_2$ systems having fully oxidized surfaces are naturally stable against surface oxidization and degradation, making them more promising for practical applications.

SUMMARY AND OUTLOOK

We have presented a concise updated review of computational design of 2D topological materials, based on discrete lattice models, focusing on two specific materials systems of 2D metalorganic frameworks and metal overlayers grown on semiconductor substrates. While many theoretical designs have been made in past few years, however, only a limited few has been confirmed experimentally. Therefore, future breakthroughs may have to come from experimental works, which are likely to be guided by computational design of material systems considered with high feasibility for experimental synthesis and characterization. In this regard, surface-based 2D topological materials appear very promising and deserve further attention, because many advanced thin film growth techniques and technologies are already in place. Furthermore, in our perspective, currently there are two main challenges in the field of topological materials, one is to increase the gap to realize high temperature topological state, and the other is to separate topological boundary state from bulk state in a transport measurement. The former challenge could be met by designing systems with high concentration of heavy metal atoms of large SOC, while the latter requires more innovative materials designs. One very interesting latest development is the proposal of nanostructured topological materials,[107] such as a novel form of 2D TI made of an array of identical Bi nanotubes. It has been shown that topological order makes the 'bulk' tubes in the middle of the array insulating, whereas the 'boundary' tubes outside conducting.[95] This distinction between the bulk and boundary tubes provides a significant advantage in terms of eliminating the bulk contribution to the quantized boundary transport, because it is much easier to address individual tubes than atom rows by placing electrodes only on a few conducting boundary tubes. This may open a completely new avenue of topological materials by extending topological phases into a wide range of unknown nanomaterials to be explored.

Finally, we think one understudied area is the computational design of topological materials in strongly correlated systems, which requires development and application of computational methods beyond standard DFT. In this regard, organic topological materials provide an ideal platform for material realization of lattice Hamiltonians of topological states with different forms and degrees of electron–electron correlation, because the organometallic framework is highly tunable with different choices of metals made of p-, d-, or f-orbitals to tune the level of charge localization, and with different lattice symmetries and ligand molecules to tune the interaction range and strength. We also note that topological superconductors[108,109] have drawn much recent attention.

ACKNOWLEDGMENTS

Z.F.W. acknowledges support from the NSFC (Grant No. 21603210), Chinese Youth 1000 Talents Program, and Fundamental Research Funds for the Central Universities. K.H.J. and F.L. acknowledge support from US Department of Energy - Basic Energy Sciences (Grant No. DE-FG02-04ER46148).

REFERENCES

1. Kohn W, Sham LJ. Self-consistent equations including exchange and correlation effects. *Phys Rev A* 1965, 140:1133.
2. Alder BJ, Wainwright TE. Studies in molecular dynamics. I. General method. *J Chem Phys* 1959, 31:459–466.
3. Binder K. *The Monte Carlo Method in Condensed Matter Physics*. New York, NY: Springer; 1995.
4. Chen LQ. Phase-field models for microstructure evolution. *Annu Rev Mater Res* 2002, 32:113.
5. Dingreville R, Karnesky RA, Puel G, Schmitt J-H. Review of the synergies between computational

modeling and experimental characterization of materials across length scales. *J Mater Sci* 2016, 51:1178–1203.

6. Yang K, Setyawan W, Wang S, Nardelli MB, Curtarolo S. A search model for topological insulators with high-throughput robustness descriptors. *Nat Mater* 2012, 11:614–619.
7. Curtarolo S, Hart GLW, Nardelli MB, Mingo N, Sanvito S, Levy O. The high-throughput highway to computational materials design. *Nat Mater* 2013, 12:191–201.
8. Liu Z, Liu F, Wu Y-S. Exotic electronic states in the world of flat bands: from theory to material. *Chin Phys B* 2014, 23:077308.
9. Kane CL, Mele EJ. Quantum spin Hall effect in graphene. *Phys Rev Lett* 2005, 95:226801.
10. Bernevig BA, Hughes TL, Zhang S-C. Quantum spin Hall effect and topological phase transition in HgTe quantum wells. *Science* 2006, 314:1757–1761.
11. Königl M, Wiedmann S, Brüne C, Roth A, Buhmann H, Molenkamp LW, Qi X-L, Zhang S-C. Quantum spin Hall insulator state in HgTe quantum wells. *Science* 2007, 318:766–770.
12. Hasan MZ, Kane CL. Topological insulators. *Rev Mod Phys* 2010, 82:3045–3067.
13. Qi X-L, Zhang S-C. Topological insulators and superconductors. *Rev Mod Phys* 2011, 83:1057–1110.
14. Bansil A, Lin H, Das T. Topological band theory. *Rev Mod Phys* 2016, 88:021004.
15. Yennie DR. Integral quantum Hall effect for nonspecialists. *Rev Mod Phys* 1987, 59:781–824.
16. Huckestein B. Scaling theory of the integer quantum Hall effect. *Rev Mod Phys* 1995, 67:357–396.
17. Ren Y, Qiao Z, Niu Q. Topological phases in two-dimensional materials: a review. *Rep Prog Phys* 2016, 79:066501.
18. Wang ZF, Liu Z, Liu F. Organic topological insulators in organometallic lattices. *Nat Commun* 2013, 4:1471.
19. Wang ZF, Su N, Liu F. Prediction of a two-dimensional organic topological insulator. *Nano Lett* 2013, 13:2842–2845.
20. Zhang L, Wang ZF, Huang B, Cui B, Wang ZMM, Du S, Gao HJ, Liu F. Intrinsic two-dimensional organic topological insulators in metal-DCA lattices. *Nano Lett* 2016, 16:2072–2075.
21. Zhou M, Ming W, Liu Z, Wang ZF, Li P, Liu F. Epitaxial growth of large-gap quantum spin Hall insulator on semiconductor surface. *Proc Natl Acad Sci U S A* 2014, 111:14378–14381.
22. Wang ZF, Jin K-H, Liu F. Quantum spin Hall phase in 2D trigonal lattice. *Nat Commun* 2016, 7:12746.
23. Wang ZF, Zhang H, Liu D, Liu C, Tang C, Song C, Zhong Y, Peng J, Li F, Nie C, et al. Topological edge states in a high-temperature superconductor FeSe/$SrTiO_3$(001) film. *Nat Mater* 2016, 15:968–973.
24. Fu L, Kane CL. Topological insulators with inversion symmetry. *Phys Rev B* 2007, 76:045302.
25. Haldane FDM. Model for a quantum Hall effect without Landau levels: condensed-matter realization of the "parity anomaly". *Phys Rev Lett* 1988, 61:2015–2018.
26. Weeks C, Hu J, Alicea J, Franz M, Wu R. Engineering a robust quantum spin Hall state in graphene via adatom deposition. *Phys Rev X* 2011, 1:021001.
27. Liu CC, Feng W, Yao Y. Quantum spin Hall effect in silicene and two-dimensional germanium. *Phys Rev Lett* 2011, 107:076802.
28. Xu Y, Yan B, Zhang H-J, Wang J, Xu G, Tang P, Duan W, Zhang S-C. Large-gap quantum spin Hall insulators in tin films. *Phys Rev Lett* 2013, 111:136804.
29. Kou L, Yan B, Hu F, Wu S-C, Wehling TO, Felser C, Chen C, Frauenheim T. Graphene-based topological insulator with an intrinsic bulk band gap above room temperature. *Nano Lett* 2013, 13:6251–6255.
30. Chuang F-C, Yao L-Z, Huang Z-Q, Liu Y-T, Hsu C-H, Das T, Lin H, Bansil A. Prediction of large-gap two-dimensional topological insulators consisting of bilayers of group III elements with Bi. *Nano Lett* 2014, 14:2505–2508.
31. Si C, Liu J, Xu Y, Wu J, Gu B-L, Duan W. Functionalized germanene as a prototype of large-gap two-dimensional topological insulators. *Phys Rev B* 2014, 89:115429.
32. Song Z, Liu C-C, Yang J, Han J, Ye M, Fu B, Yang Y, Niu Q, Lu J, Yao Y. Quantum spin Hall insulators and quantum valley Hall insulators of BiX/SbX (X = H, F, Cl and Br) monolayers with a record bulk band gap. *NPG Asia Mater* 2014, 6:147.
33. Ma Y, Dai Y, Kou L, Frauenheim T, Heine T. Robust two-dimensional topological insulators in methyl-functionalized bismuth, antimony, and lead bilayer films. *Nano Lett* 2015, 15:1083–1089.
34. Zhao M, Zhang X, Li L. Strain-driven band inversion and topological aspects in antimonene. *Sci Rep* 2015, 5:16108.
35. Jin K-H, Jhi S-H. Quantum anomalous Hall and quantum spin-Hall phases in flattened Bi and Sb bilayers. *Sci Rep* 2015, 5:8426.
36. Yang F, Miao L, Wang ZF, Yao M-Y, Zhu F, Song YR, Wang M-X, Xu J-P, Fedorov AV, Sun Z, et al. Spatial and energy distribution of topological edge states in single Bi(111) bilayer. *Phys Rev Lett* 2012, 109:016801.
37. Drozdov IK, Alexandradinata A, Jeon S, Nadj-Perge S, Ji H, Cava RJ, Bernevig BA, Yazdani A.

One-dimensional topological edge states of bismuth bilayers. *Nat Phys* 2014, 10:664–669.

38. Kim SH, Jin K-H, Park J, Kim JS, Jhi S-H, Kim T-H, Yeom HW. Edge and interfacial states in a two-dimensional topological insulator: Bi(111) bilayer on Bi_2Te_2Se. *Phys Rev B* 2014, 89:155436.
39. Knez I, Du R-R, Sullivan G. Evidence for helical edge modes in inverted InAs/GaSb quantum wells. *Phys Rev Lett* 2011, 107:136603.
40. Qi X-L, Hughes TL, Zhang S-C. Topological field theory of time-reversal invariant insulators. *Phys Rev B* 2008, 78:195424.
41. Hsieh D, Qian D, Wray L, Xia Y, Hor YS, Cava RJ, Hasan MZ. A topological Dirac insulator in a quantum spin Hall phase. *Nature* 2008, 452:970–974.
42. Zhang HJ, Liu CX, Qi X-L, Dai X, Fang Z, Zhang S-C. Topological insulators in Bi_2Se_3, Bi_2Te_3 and Sb_2Te_3 with a single Dirac cone on the surface. *Nat Phys* 2009, 5:438–442.
43. Hsieh D, Xia Y, Wray L, Qian D, Pal A, Dil JH, Osterwalder J, Meier F, Bihlmayer G, Kane CL, et al. Observation of unconventional quantum spin textures in topological insulators. *Science* 2009, 323:919–922.
44. Xia Y, Qian D, Hsieh D, Wray L, Pal A, Lin H, Bansil A, Grauer D, Hor YS, Cava RJ, et al. Observation of a large-gap topological insulator class with a single Dirac cone on the surface. *Nat Phys* 2009, 5:398–402.
45. Chen YL, Analytis JG, Chu J-H, Liu ZK, Mo S-K, Qi XL, Zhang HJ, Lu DH, Dai X, Fang Z, et al. Experimental realization of a three-dimensional topological insulator, Bi_2Te_3. *Science* 2009, 325:178–180.
46. Chen YL, Chu J-H, Analytis JG, Liu ZK, Igarashi K, Kuo H-H, Qi XL, Mo SK, Moore RG, Lu DH, et al. Massive Dirac fermion on the surface of a magnetically doped topological insulator. *Science* 2010, 329:659–662.
47. Wang ZF, Liu Z, Liu F. Quantum anomalous Hall effect in 2D organic topological insulators. *Phys Rev Lett* 2013, 110:196801.
48. Liu Z, Wang ZF, Mei JW, Wu YS, Liu F. Flat Chern band in a two-dimensional organometallic framework. *Phys Rev Lett* 2013, 110:106804.
49. Kambe T, Sakamoto R, Kusamoto T, Pal T, Fukui N, Hoshiko K, Shimojima T, Wang Z, Hirahara T, Ishizaka K, et al. Redox control and high conductivity of nickel bis(dithiolene) complex π-nanosheet: a potential organic two-dimensional topological insulator. *J Am Chem Soc* 2014, 136:14357–14360.
50. Zhang X, Zhao M. Prediction of quantum anomalous Hall effect on graphene nanomesh. *RSC Adv* 2015, 5:9875–9880.
51. Ma Y, Dai Y, Li X, Sun Q, Huang B. Prediction of two-dimensional materials with half-metallic Dirac cones: $Ni_2C_{18}H_{12}$ and $Co_2C_{18}H_{12}$. *Carbon* 2014, 73:382–388.
52. Zhang X, Wang Z, Zhao M, Liu F. Tunable topological states in electron-doped HTT-Pt. *Phys Rev B* 2016, 93:165401.
53. Zhang X, Zhao M. Robust half-metallicity and topological aspects in two-dimensional Cu-TPyB. *Sci Rep* 2015, 5:14098.
54. Wei L, Zhang X, Zhao M. Spin-polarized Dirac cones and topological nontriviality in a metal-organic framework $Ni_2C_{24}S_6H_{12}$. *Phys Chem Chem Phys* 2016, 18:8059–8064.
55. Kim H-J, Li C, Feng J, Cho J-H, Zhang Z. Competing magnetic orderings and tunable topological states in two-dimensional hexagonal organometallic lattices. *Phys Rev B* 2016, 93:041404(R).
56. Dong L, Kim Y, Er D, Rappe AM, Shenoy VB. Two-dimensional π-conjugated covalent-organic frameworks as quantum anomalous Hall topological insulators. *Phys Rev Lett* 2016, 116:096601.
57. Wu C, Sarma SD. $p_{x,y}$-orbital counterpart of graphene: cold atoms in the honeycomb optical lattice. *Phys Rev B* 2008, 77:235107.
58. Grohol D, Matan K, Cho J-H, Lee S-H, Lynn JW, Nocera DG, Lee YS. Spin chirality on a two-dimensional frustrated lattice. *Nat Mater* 2005, 4:323–328.
59. Han T, Helton JS, Chu S, Nocera DG, Rodriguez-Rivera JA, Broholm C, Lee YS. Fractionalized excitations in the spin-liquid state of a kagome-lattice antiferromagnet. *Nature* 2012, 492:406–410.
60. Zhu W, Gong SS, Sheng DN. Interaction-driven fractional quantum Hall state of hard-core bosons on kagome lattice at one-third filling. *Phys Rev B* 2016, 94:035129.
61. Kambe T, Sakamoto R, Hoshiko K, Takada K, Miyachi M, Ryu J-H, Sasaki S, Kim J, Nakazato K, Takata M, et al. π-Conjugated nickel bis(dithiolene) complex nanosheet. *J Am Chem Soc* 2013, 135:2462–2465.
62. Pawin G, Wong KL, Kim D, Sun D, Bartels L, Hong S, Rahman TS, Carp R, Marsella M. A surface coordination network based on substrate-derived metal adatoms with local charge excess. *Angew Chem Int Ed* 2008, 47:8442–8445.
63. Murakami S. Quantum spin Hall effect and enhanced magnetic response by spin-orbit coupling. *Phys Rev Lett* 2006, 97:236805.
64. Liu Z, Liu C-X, Wu Y-S, Duan W, Liu F. Stable nontrivial Z_2 topology in ultrathin Bi (111) films: a first-principles study. *Phys Rev Lett* 2011, 107:136805.

65. Wang ZF, Chen L, Liu F. Tuning topological edge states of Bi (111) bilayer film by edge adsorption. *Nano Lett* 2014, 14:2879–2883.
66. Chen L, Wang ZF, Liu F. Robustness of two-dimensional topological insulator states in bilayer bismuth against strain and electrical field. *Phys Rev B* 2013, 87:235420.
67. Miao L, Wang ZF, Ming W, Yao M-Y, Wang M, Yang F, Song YR, Zhu F, Fedorov AV, Sun Z, et al. *Proc Natl Acad Sci U S A* 2013, 110:2758–2763.
68. Wang ZF, Yao M-Y, Ming W, Miao L, Zhu F, Liu C, Gao CL, Qian D, Jia J-F, Liu F. Creation of helical Dirac fermions by interfacing two gapped systems of ordinary fermions. *Nat Commun* 2013, 4:1384.
69. Zhou M, Ming W, Liu Z, Wang ZF, Yao Y, Liu F. Formation of quantum spin Hall state on Si surface and energy gap scaling with strength of spin orbit coupling. *Sci Rep* 2014, 4:7102.
70. Zhou M, Liu Z, Ming W, Wang ZF, Liu F. sd^2 graphene: kagome band in hexagonal lattice. *Phys Rev Lett* 2014, 113:236802.
71. Wang ZF, Liu F. Self-assembled Si (111) surface states: 2D Dirac material for THz plasmonics. *Phys Rev Lett* 2015, 115:026803.
72. Hsu C-H, Huang Z-Q, Chuang F-C, Kuo C-C, Liu Y-T, Lin H, Bansil A. The nontrivial electronic structure of Bi/Sb honeycombs on SiC(0001). *New J Phys* 2015, 17:025005.
73. Crisostomo CP, Yao L-Z, Huang Z-Q, Hsu C-H, Chuang F-C, Lin H, Albao MA, Bansil A. Robust large gap two-dimensional topological insulators in hydrogenated III-V buckled honeycombs. *Nano Lett* 2015, 15:6568–6574.
74. Xu Y, Tang P, Zhang S-C. Large-gap quantum spin Hall states in decorated stanene grown on a substrate. *Phys Rev B* 2015, 92:081112(R).
75. Liang Q-F, Yu R, Zhou J, Hu X. Topological states of non-Dirac electrons on a triangular lattice. *Phys Rev B* 2016, 93:035135.
76. Chuang F-C, Hsu C-H, Chou H-L, Crisostomo CP, Huang Z-Q, Wu S-Y, Kuo C-C, Yeh W-CV, Lin H, Bansil A. Prediction of two-dimensional topological insulator by forming a surface alloy on Au/Si(111) substrate. *Phys Rev B* 2016, 93:035429.
77. Bian G, Wang Z, Wang X-X, Xu C, Xu S, Miller T, Hasan MZ, Liu F, Chiang T-C. Engineering electronic structure of a two-dimensional topological insulator Bi(111) bilayer on Sb nanofilms by quantum confinement effect. *ACS Nano* 2016, 10:3859–3864.
78. Zhou J, Sun Q, Wang Q, Kawazoe Y, Jena P. Intrinsic quantum spin Hall and anomalous Hall effects in h-Sb/Bi epitaxial growth on a ferromagnetic MnO_2 thin film. *Nanoscale* 2016, 8:11202–11209.
79. Huang B, Jin K-H, Zhuang HL, Zhang L, Liu F. Interface orbital engineering of large-gap topological states: decorating gold on a Si(111) surface. *Phys Rev B* 2016, 93:115117.
80. Li P, Zhou M, Zhang L, Guo Y, Liu F. Formation of a quantum spin Hall state on a Ge(111) surface. *Nanotech* 2016, 27:095703.
81. Dev BN, Aristov V, Hertel N, Thundat T, Gibson WM. Chemisorption of bromine on cleaved silicon (111) surfaces: an X-ray standing wave interference spectrometric analysis. *Surf Sci* 1985, 163:457–477.
82. Gruznev DV, Bondarenko LV, Matetskiy AV, Yakovlev AA, Tupchaya AY, Eremeev SV, Chulkov EV, Chou J-P, Wei C-M, Lai M-Y, et al. A strategy to create spin-split metallic bands on silicon using a dense alloy layer. *Sci Rep* 2014, 4:4742.
83. Nakatsuji K, Motomura Y, Niikura R, Komori F. Selective doping in a surface band and atomic structures of the Ge(111)-Au surface. *J Phys Condens Matter* 2013, 25:045007.
84. Hilner E, Mikkelsen A, Eriksson J, Andersen JN, Lundgren E, Zakharov A, Yi H, Kratzer P. Au wetting and nanoparticle stability on GaAs(111)B. *Appl Phys Lett* 2006, 89:251912.
85. Fedorov AV, Verbitskiy NI, Haberer D, Struzzi C, Petaccia L, Usachov D, Vilkov OY, Vyalikh DV, Fink J, Knupfer M, et al. Observation of a universal donor-dependent vibrational mode in graphene. *Nat Commun* 2014, 5:3257.
86. Miyata Y, Nakayama K, Sugawara K, Sato T, Takahashi T. High-temperature superconductivity in potassium-coated multilayer FeSe thin films. *Nat Mater* 2015, 14:775–779.
87. Hao N, Hu J. Topological phases in the single-layer FeSe. *Phys Rev X* 2014, 4:031053.
88. Wang Z, Zhang P, Xu G, Zeng LK, Miao H, Xu X, Qian T, Weng H, Richard P, Fedorov AV, et al. Topological nature of the $FeSe_{0.5}Te_{0.5}$ superconductor. *Phys Rev B* 2015, 92:115119.
89. Hao N, Shen S-Q. Topological superconducting states in monolayer $FeSe/SrTiO_3$. *Phys Rev B* 2015, 92:165104.
90. Xu G, Lian B, Tang P, Qi X-L, Zhang S-C. Topological superconductivity on the surface of Fe-based superconductors. *Phys Rev Lett* 2016, 117:047001.
91. Liu D, Zhang W, Mou D, He J, Ou Y-B, Wang Q-Y, Li Z, Wang L, Zhao L, He S, et al. Electronic origin of high-temperature superconductivity in single-layer FeSe superconductor. *Nat Commun* 2012, 3:931.
92. He S, He J, Zhang W, Zhao L, Liu D, Liu X, Mou D, Ou Y-B, Wang Q-Y, Li Z, et al. Phase diagram and electronic indication of high-temperature superconductivity at 65 K in single-layer FeSe films. *Nat Mater* 2013, 12:605–610.

93. Tan S, Zhang Y, Xia M, Ye Z, Chen F, Xie X, Peng R, Xu D, Fan Q, Xu H, et al. Interface-induced superconductivity and strain-dependent spin density waves in FeSe/$SrTiO_3$ thin films. *Nat Mater* 2013, 12:634–640.
94. Guo H, Feng S, Shen SQ. Quantum spin Hall effect induced by nonmagnetic and magnetic staggered potentials. *Phys Rev B* 2011, 83:045114.
95. Wang QH, Kalantar-Zadeh K, Kis A, Coleman JN, Strano MS. Electronics and optoelectronics of two-dimensional transition metal dichalcogenides. *Nat Nano* 2012, 7:699–712.
96. Qian X, Liu J, Fu L, Li J. Quantum spin Hall effect in two-dimensional transition metal dichalcogenides. *Science* 2014, 346:1344–1347.
97. Cazalilla MA, Ochoa H, Guinea F. Quantum spin Hall effect in two-dimensional crystals of transition-metal dichalcogenides. *Phys Rev Lett* 2014, 113:077201.
98. Choe D-H, Sung H-J, Chang KJ. Understanding topological phase transition in monolayer transition metal dichalcogenides. *Phys Rev B* 2016, 93:125109.
99. Nie SM, Song Z, Weng H, Fang Z. Quantum spin Hall effect in two-dimensional transition-metal dichalcogenide haeckelites. *Phys Rev B* 2015, 91:235434.
100. Ma Y, Kou L, Li X, Dai Y, Smith SC, Heine T. Quantum spin Hall effect and topological phase transition in two-dimensional square transition-metal dichalcogenides. *Phys Rev B* 2015, 92:085427.
101. Sun Y, Felser C, Yan B. Graphene-like Dirac states and quantum spin Hall insulators in square-octagonal MX_2 (M = Mo, W; X = S, Se, Te) isomers. *Phys Rev B* 2015, 92:165421.
102. Ma Y, Kou L, Li X, Dai Y, Heine T. Two-dimensional transition metal dichalcogenides with a hexagonal lattice: room-temperature quantum spin Hall insulators. *Phys Rev B* 2016, 93:035442.
103. Shitade A, Katsura H, Kuneš J, Qi X-L, Zhang S-C, Nagaosa N. Quantum spin Hall effect in a transition metal oxide Na_2IrO_3. *Phys Rev Lett* 2009, 102:256403.
104. Zhou L, Kou L, Sun Y, Felser C, Hu F, Shan G, Smith SC, Yan B, Frauenheim T. New family of quantum spin Hall insulators in two-dimensional transition-metal halide with large nontrivial band gaps. *Nano Lett* 2015, 15:7867–7872.
105. Weng H, Ranjbar A, Liang Y, Song Z, Khazaei M, Yunoki S, Arai M, Kawazoe Y, Fang Z, Dai X. Large-gap two-dimensional topological insulator in oxygen functionalized MXene. *Phys Rev B* 2015, 92:075436.
106. Si C, Jin K-H, Zhou J, Sun Z, Liu F. Large-gap quantum spin Hall state in MXenes: *d*-band topological order in a triangular lattice. *Nano Lett* 2016, 16:6584–6591.
107. Jin K-H, Jhi S-H, Liu F. Private communication.
108. Leijnse M, Flensberg K. Introduction to topological superconductivity and Majorana fermions. *Semicond Sci Technol* 2012, 27:124003.
109. Beenakker CWJ. Random-matrix theory of Majorana fermions and topological superconductors. *Rev Mod Phys* 2015, 87:1037–1066.

